Journal Pre-proofs

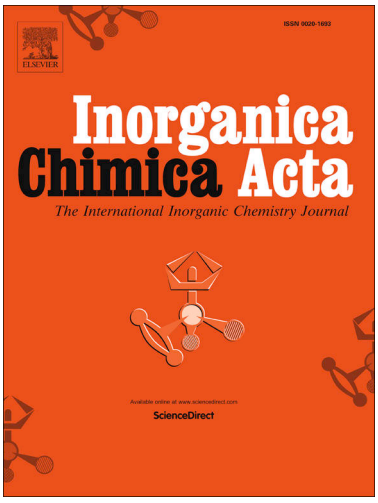

Research paper

Two novel copper(II) salamo-based complexes: Syntheses, X-ray crystal structures, spectroscopic properties and Hirshfeld surfaces analyses

Meng Yu, Yu Zhang, Ying-Qi Pan, Li Wang

PII: S0020-1693(20)30521-1
DOI: https://doi.org/10.1016/j.ica.2020.119701
Reference: ICA 119701

To appear in: *Inorganica Chimica Acta*

Received Date: 18 March 2020
Revised Date: 24 April 2020
Accepted Date: 24 April 2020

Please cite this article as: M. Yu, Y. Zhang, Y-Q. Pan, L. Wang, Two novel copper(II) salamo-based complexes: Syntheses, X-ray crystal structures, spectroscopic properties and Hirshfeld surfaces analyses, *Inorganica Chimica Acta* (2020), doi: https://doi.org/10.1016/j.ica.2020.119701

Two novel copper(II) salamo-based complexes: Syntheses, X-ray crystal structures, spectroscopic properties and Hirshfeld surfaces analyses

Meng Yu, Yu Zhang, Ying-Qi Pan, Li Wang*

School of Chemical and Biological Engineering, Lanzhou Jiaotong University, Lanzhou, Gansu 730070, PR China

A B S T R A C T

Two novel Cu(II) complexes, $[\{Cu(L^1)\}_2(CH_3OH)]\cdot CH_3OH$ (**1**) and $[Cu(L^2)_2]$ (**2**) derived from a half-salamo-based N_2O-donor ligand (HL: 2-[*O*-(1-ethyloxyamide)]oxime-4-nitrophenol) were synthesized and characterized by elemental analyses, infrared spectroscopy, ultraviolet-visible absorption spectroscopy, X-ray single crystal diffraction and Hirshfeld surfaces analyses. Here, ligands H_2L^1 (4,4′-Dinitro-2,2′-[ethylenedioxybis(nitrilomethylidyne)]diphenol) and HL^2 ((E)-2-Hydroxy-5-nitrobenzaldehyde *O*-(2-((propan-2-ylideneamino)oxy)ethyl) oxime) are obtained by rearrangement reaction due to the catalysis of Cu(II) ion during the formation of the complexes **1** and **2**. The complex **1** consists of two Cu(II) ions, two fully deprotonated ligand $(L^1)^-$ units, one coordinated methanol and one crystallized methanol molecules, forming an novel unsymmetric dinuclear structure previously unreported, and possesses an infinite 3D supramolecular structure. The Cu(II) ions are penta-coordinated and with distorted tetragonal pyramidal geometric configuration. The complex **2** is an novel symmetric mononuclear structure, consists of one Cu(II) ion, two fully deprotonated ligand $(L^2)^-$ units, forming a four-coordinated planar quadrilateral

* Corresponding authors. Tel.: +86 931 4938703; fax: +86 931 4938795.

E-mail addresses: wangli_78@126.com (L. Wang).

geometric configuration with a Cu(II) ion occupying the center of symmetry, and possesses an infinite 2D supramolecular structure. Simultaneously, the fluorescence properties and Hirshfeld surfaces analyses of the Cu(II) complexes **1** and **2** were also investigated.

Keywords: Salamo-based ligand; Cu(II) complex; Synthesis; Crystal structure; Hirshfeld surface analysis

1. Introduction

It is common knowledge that salen-based Schiff base compounds (R–CH=N–$(CH_2)_2$–N=CH–R) are a very important kind of versatile chelating ligands [1,2], which has long been a research hotspot on coordination chemistry. Because these ligands have a N_2O_2 tetradentate coordinate environment [3–4], and the N_2O_2 tetradentate moiety can coordinate with divalent *d*-block metal ions to obtain neutral metal complexes thus capable of forming a lot of kinds of stable metal(II) complexes having different structures and properties [5–8]. The two phenolic O–H groups of the ligand H_2L^1 in the N_2O_2 metal complexes are converted into more polarized O–M (phenoxo-metal) bonds, and lead to negatively charged phenoxy groups. Because of the negative charge, the phenoxy groups can further coordinate to d-block transition metal. Among these salen-based transition metal(II) complexes, some have been explored in biological fields [9–11], electrochemical conducts [12], nonlinear optical materials [13,14], molecular recognitions [15], magnetic materials [16,17], luminescence properties [18,19] and supra-molecular architectures [20–24] and so on.

Derivatives as salan-based ligands, in recent years, our research mostly concentrated on the syntheses of salamo-based ligands [25–32]. These ligands belong to oxime-type compounds, which are different from salan-based Schiff base compounds. Their metal complexes have been investigated in forming transition metal(II) complexes [33–36] with interesting properties, some works have been devoted to synthesize and characterize mono- [37–39], di- and multi-nuclear metal(II)

complexes bearing salamo-based ligands and their derivatives [40–43]. At present, there are few studies on half-salamo-based ligands, Herein, as part of our ongoing interest in salamo-based complexes, X-ray crystal structures, spectroscopic properties and Hirshfeld surfaces analyses of two newly designed and synthesized Cu(II) complexes, $[\{Cu(L^1)\}_2(CH_3OH)]\cdot CH_3OH$ (**1**) and $[Cu(L^2)_2]$ (**2**) derived from a half-salamo-based ligand HL have been investigated in detail.

2. **Experimental**

2.1. Materials and Physical Measurements

5-Nitrosalicylic aldehyde of 99% purity was purchased from Alfa Aesar and used without further purification. The other reagents and solvents were analytical grade reagents from Tianjin Chemical Reagent Factory.

C, H and N analyses were obtained using a GmbH VarioEL V3.00 automatic elemental analyzer. Elemental analysis for Cu(II) was conducted using an IRIS ER/S·WP^{-1} ICP atomic emission spectrometer. ^{1}H NMR spectra were recorded using a Bruker AVANCE DRX-400 spectrometer. The melting points were determined by microscopic melting point instrument made in Beijing Tektronix Instruments Limited Company. IR spectra were recorded on a VERTEX70 FT-IR spectrophotometer, with samples prepared as KBr (500–4000 cm^{-1}) and CsI (100–500 cm^{-1}) pellets. UV/Vis absorption spectra were recorded on a Shimadzu UV-2550 spectrometer. X-ray single crystal structure determinations were carried out on a Bruker Smart Apex CCD diffractometer. Hirshfeld surfaces analyses of the Cu(II) complexes were performed using the Crystal Explorer program were all made according to similar methods previously reported [30,38]. Fluorescence spectra were recorded on an F-7000 FL spectrophotometer.

2.2. Preparation of the ligand HL

The major reaction step involved in the synthesis of HL is given in Scheme 1. 1,2-Bis(aminooxy)ethane was synthesized following the previously reported literature

[44].

The ligand HL: 2-[*O*-(1-Ethyloxyamide)]oxime-4-nitrophenol was prepared by the solution of 5-nitrosalicylic aldehyde (3 mmol, 506.1 mg) in absolute ethanol (6 mL) was added to a solution of 1,2-bis(aminooxy)ethane (3 mmol, 272.6 mg) in absolute ethanol (6 mL). The suspension solution was stirred and refluxed at 55 °C for 6 h. The solution was concentrated in *vacuo* and the residue was purified by column chromatography (SiO_2, chloroform/ethyl acetate, 15:1) to afford light yellow flocculent crystalline solid, which was collected by suction filtration. Yield: 78.7 %. Anal. Calc. for $C_9H_{11}N_3O_5$ (%): C, 44.82; H, 4.60; N, 17.42. Found: C, 44.99; H, 4.38; N,17.30. ^{1}H NMR (400 MHz, $CDCl_3$) δ 10.72 (s, 1H), 8.27 (s, 1H), 8.17 (m, 2H), 7.07 (d, J = 9.1 Hz, 1H), 5.54 (s, 2H), 4.42 (s, 2H), 4.00 (s, 2H).

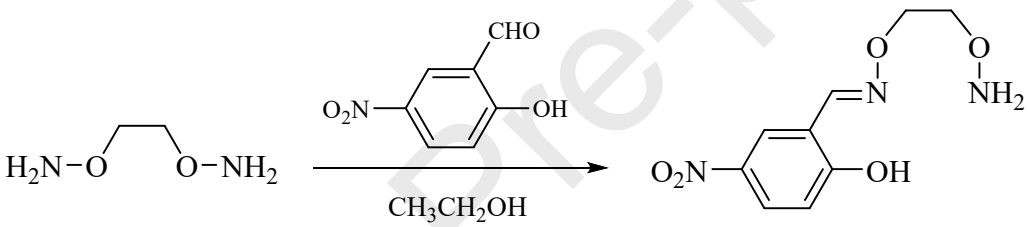

Scheme 1. Synthetic route to the ligand HL.

*2.3. Synthesis of the complex **1***

To a methanol solution (3 mL) of bis(acetylacetonato)copper(II) (7.85 mg, 0.03 mmol) was added dropwise a solution of HL (9.64 mg, 0.04 mmol) in 4 mL of dichloromethane solution, and the mixed solution color changed to light green immediately. The mixture solution was filtered and the filtrate was allowed to stand for about two weeks. Through partial solvent evaporation, single crystals suitable for X-ray diffraction analysis were obtained. Yield, 56.9%. Anal. Calc. for $[\{Cu(L^1)\}_2(CH_3OH)]\cdot CH_3OH$ ($C_{34}H_{33}Cu_2N_8O_{18}$) (%): C, 42.15; H, 3.43; N, 11.57; Cu, 13.12. Found: C, 42.37; H, 3.31; N, 11.43; Cu, 13.15.

*2.4. Synthesis of the complex **2***

To a methanol solution (4 mL) of $Cu(OAc)_2\cdot H_2O$ (3.99 mg, 0.02 mmol) was added dropwise a solution of HL (9.64 mg, 0.04 mmol) in 4 mL of acetone, and the mixed solution color changed to green immediately, a drop of DMF was added to the mixed

solution. The mixture solution was filtered and the filtrate was allowed to stand for about three weeks. Through partial solvent evaporation, single crystals suitable for X-ray diffraction analysis were obtained. Yield: 50.5%. Anal. Calc. for $[Cu(L^2)_2]$ ($C_{24}H_{28}CuN_6O_{10}$) (%): C, 46.19; H, 4.52; N, 13.47; Cu, 10.18. Found: C, 46.31; H, 4.57; N, 13.34; Cu, 10.02.

*2.5. X-ray structure determinations of the complexes **1** and **2***

The crystal diffractometer provides a monochromatic beam of Mo Kα radiation (0.071073 nm) produced using Graphite monochromator from a sealed Mo X-ray tube was used for obtaining crystal data of the complexes **1** and **2** at 173(2) and 297 K, respectively. The LP factor semi-empirical absorption corrections were applied using the SADABS program. The structures were solved by the direct methods (SHELXS-2014) [45]. All hydrogen atoms were added theoretically and difference-Fourier map revealed the positions of the remaining atoms. All non-hydrogen atoms were refined anisotropically using a full-matrix least-squares procedure on F^2 with SHELXL-2014 [45]. The crystal data and experimental parameters relevant to the structure determinations are listed in Table 1**.**

Table 1

Crystallographic data and refinement parameters for the complexes **1** and **2**.

Complex	Complex **1**	Complex **2**
Empirical formula	$C_{34}H_{33}Cu_2N_8O_{18}$	$C_{24}H_{28}CuN_6O_{10}$
Molecular weight	968.76	624.06
Crystal size (mm)	0.21 × 0.18 × 0.16	0.22 × 0.19 × 0.17
Habit	Block-shaped	Block-shaped
Crystal system	Monoclinic	Triclinic
Space group	$P2_1/C$	P-1
Unit cell dimension		
a (Å)	13.5463(11)	4.0753(15)
b (Å)	24.841(2)	13.119(3)
c (Å)	11.6264(9)	13.178(3)
α (°)	90	69.737(14)
β (°)	107.709(2)	81.10
γ (°)	90	81.06
V (Å^3)	3726.9(5)	649.0(3)
Z	4	1
D_{calc} (g · cm^{-3})	1.727	1.597

μ (mm^{-1})	1.236	0.912
F(000)	1980	323
θ range for data collection (°)	2.013 to 13	1.922 to 24.998
Index ranges	-16 ≤ h ≤ 16, -29 ≤ k ≤ 23, -13 ≤ l ≤ 13	-4 ≤ h ≤ 4, -15 ≤ k ≤ 15, -15 ≤ l ≤ 15
Reflections collected	23672	2251
Completeness to (%) (θ)	99.9 (25.008)	99 (24.998)
Data/restraints/parameters	6565/0/563	2251/0/190
Final R_1, wR_2 indices	0.01424, 0.0684	0.1886, 0.1620
R_1, wR_2 indices (all data)	0.1065, 0.1424	0.1047, 0.1886
Largest diff. peak and hole (e·Å^{-3})	0.970, -0.514	1.164, -0.596

3. Results and discussion

Di- and mono-nuclear Cu(II) complexes **1** and **2** were synthesized by the reaction of HL with bis(acetylacetonato)copper(II) and $Cu(OAc)_2 \cdot H_2O$ in mixed organic solvents, respectively (**Scheme** 2).

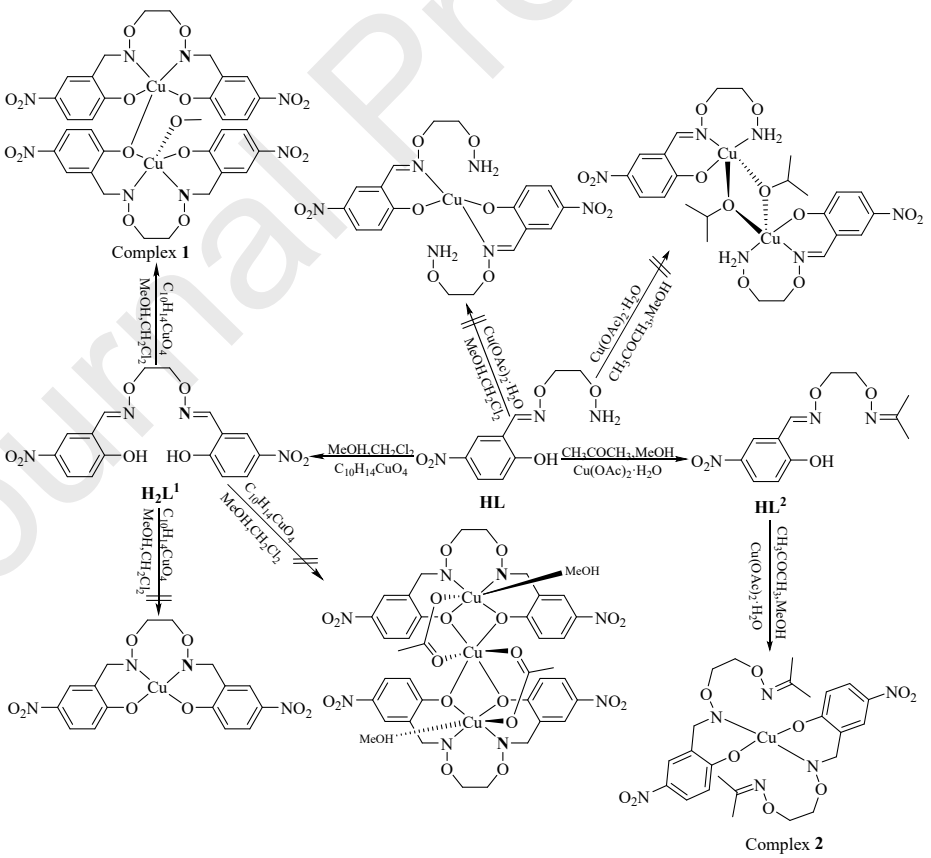

Scheme 2. Synthetic routes to the complexes **1** and **2**.

It is worth noting that a novel Cu(II) complex **1** based on a newly obtained symmetrical salamo-based ligand H_2L^1, $[\{Cu(L^1)\}_2(CH_3OH)]\cdot CH_3OH$, was gained instead of the half-salamo-based Cu(II) complex expected in advance. The results show that due to the catalysis of Cu(II) ions, complexation leads to a N-O bond cleavage in HL (make the N-O-N cavity disappear), resulting in a new symmetric N_2O_2 tetradentate ligand H_2L^1, which coordinates with Cu(II) ions and forms a novel homo-dinuclear Cu(II) complex **1**. So actually, the unexpected dinuclear Cu(II) complex **1** was formed by coordination of H_2L^1 with bis(acetylacetonato)copper(II), This structure is different from the common structures of 1:1 [33] and 2:3 [4] ($(L)^{2-}$: Cu^{2+}) reported earlier in the salamo-based metal(II) complexes.

In the process of preparing the complex **2**, $[Cu(L^2)_2]$, after adding acetone solvent to the ligand HL, another new half-salamo-based ligand HL^2 was synthesized by a Schiff base condensation of one molecule of the half-salamo-based ligand HL and one molecule of acetone by reaction. The new Cu(II) complex **2**, $[Cu(L^2)_2]$, was obtained instead of the half-salamo-based Cu(II) complex expected in advance. So actually, the unexpected mono-nuclear Cu(II) complex **2**, $[Cu(L^2)_2]$, was formed by coordination of HL^2 with Cu(II) acetate monohydrate.

The ligand HL and the complexes **1** and **2** were characterized by FT-IR, UV–vis, X-ray crystallography, fluorescence and Hirshfeld surfaces analyses. The complexes **1** and **2** are soluble in DMF, DMSO, EtOH, MeOH, CH_2Cl_2 and $CHCl_3$, but not soluble in MeCN, acetone, THF, ethyl acetate and n-hexane. Additionally, they were stable in air at room temperature.

3.1. IR Spectra analyses

The FT-IR spectra of HL and the Cu(II) complexes **1** and **2** exhibit various bands in the 4000–400 cm^{-1} region (Table 2). The hydroxyl group of HL exhibits a characteristic absorption band at 3448 cm^{-1}, an absorption band of the coordinated and crystallized methanol molecules is observed at about 3443 cm^{-1} in the complex **1**. The free ligand HL exhibits a characteristic C=N stretching band at about 1616 cm^{-1}, while $\nu_{C=N}$ bands of the Cu(II) complexes **1** and **2** are observed at about 1613 and 1605 cm^{-1}, respectively [46]. The shifts of this C=N absorption band by about 3 and 11 cm^{-1} on

going from the free ligand HL to the Cu(II) complexes **1** and **2**, respectively. The free ligand HL also exhibits a typical Ar–O stretching frequency at about 1280 cm^{-1}, while those of the Cu(II) complexes **1** and **2** appear at about 1272 and 1247 cm^{-1}, respectively [47]. The Ar–O stretching frequencies of phenoxy groups are shifted to low frequencies, which could be evidence of the Cu–O bond formation between the Cu(II) atoms and the oxygen atoms of phenoxy groups [48].

Table 2

The major IR spectral data of HL and the complexes **1** and **2** (cm^{-1}).

Compound	$\nu_{(O-H)}$	$\nu_{(C=N)}$	$\nu_{(Ar-O)}$	$\nu_{(M-O)}$	$\nu_{(M-N)}$
HL	3448	1616	1280	–	–
Complex **1**	3443	1613	1272	437	557
Complex **2**	–	1605	1247	421	525

The far-IR spectra (500-100 cm^{-1}) of the Cu(II) complexes **1** and **2** were also obtained so as to identify the bonds of Cu–O and Cu–N frequencies. The bands at about 437 and 421 cm^{-1} in the Cu(II) complexes **1** and **2** can be attributed to ν_{Cu-O}, while the bands at 557 and 525 cm^{-1} are assigned to ν_{Cu-N}, respectively [8,42].

3.2. UV-Vis absorption spectral analyses

The UV–Vis absorption spectra of the free ligand HL with the Cu(II) complexes **1** and **2** in the ethanol solution (1.0×10^{-5} mol/L) at 298 K are shown in Fig. 1. It can be seen that the absorption peaks of the Cu(II) complexes **1** and **2** are obviously different from those of HL upon complexation. Obviously, the absorption peaks of the free ligand HL differ from those of the Cu(II) complexes **1** and **2**. The absorption spectrum of the free ligand HL consists of two relatively intense peaks centered at approximate 267 and 303 nm. The absorption peak at approximate 267 nm can be assigned to the π-π* transition of the phenyl rings, and another absorption peak at approximate 303 nm can be attributed to the intra-ligand π-π* transition of the oxime groups [42]. When compared with the free ligand HL, the two absorption peaks are disappeared from the UV-vis spectra of the complexes **1** and **2**, and new absorption peaks are observed at

approximate 293 and 354 nm for the complexes **1** and **2**, and are assigned to L→M (LMCT) or M→L (MLCT) charge transition which is characteristic of the transition metal complexes with N_2O_2 coordination sphere [49].

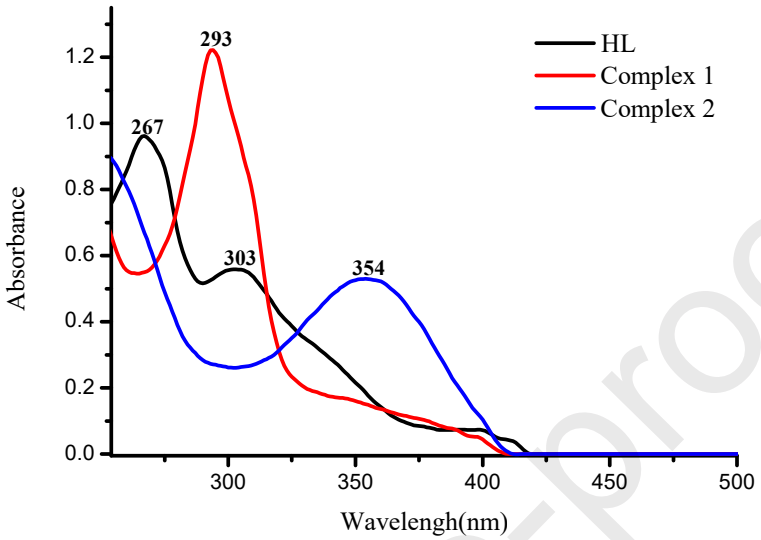

Fig. 1. UV–vis spectra of HL and the Cu(II) complexes **1** and **2** (nm).

3.3. Fluorescence properties

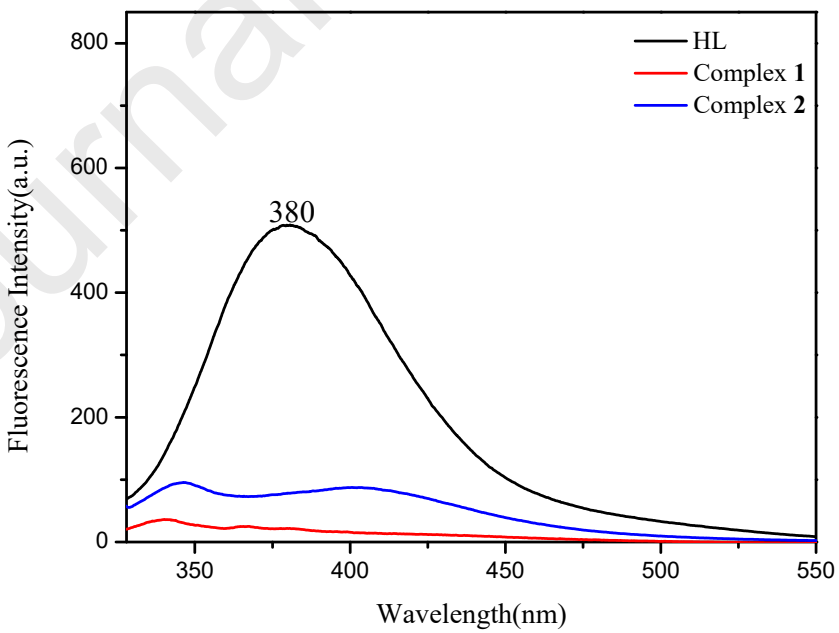

Fig. 2. Emission spectra of HL (c = 1 × 10^{-5} M, λex = 275 nm) and the complexes **1** and **2**.

The fluorescence properties of HL and the Cu(II) complexes **1** and **2** were studied, and are depicted in Fig. 2. The ligand HL displays a strong emission peak at *ca.* 380 nm upon excitation at 275 nm, and it should be attributed to the intra-ligand π–π* transition. The Cu(II) complexes **1** and **2** display lower photoluminescence compared with HL, emission intensities of the Cu(II) complexes **1** and **2** evidently are reduced, showing that the Cu(II) ions possess a certain degree of fluorescence quenching, which makes the conjugated system larger.

*3.4. Description of the crystal structure of the Cu(II) complexes **1** and **2***

X-ray crystallographic analyses reveal that the Cu(II) complexes **1** and **2** form two different forms of crystal structures, which are different from common structures of salamo-based complexes reported earlier [50–55]. The crystal structures of the Cu(II) complexes **1** and **2** and the coordination polyhedra of the Cu(II) atoms are shown in Figs. 3 and 6. Selected bond lengths and angles are listed in Tables 3 and 4**.**

*3.4.1. Crystal structure of the complex **1***

As shown in Fig. 3, in the crystal structure, the Cu(II) complex **1** consists of two Cu(II) ions, two fully deprotonated ligand $(L^1)^-$ units, one coordinated methanol and one crystallized methanol molecules. The Cu(II) complex **1** possesses an novel unsymmetrical dinuclear structure. The five-coordinated Cu atom (Cu1) lies in the N_2O_2 coordination sphere (N2, N3, O2 and O6) of the completely deprotonated ligand $(L^1)^-$ unit, and coordinated further to one oxygen atom (O14) from aother $[(L^1)Cu(CH_3OH)]$ moity, forming a distorted tetragonal pyramidal geometric configuration. Unlike the Cu1 atom, the another five-coordinated Cu atom (Cu2) in $[(L^1)Cu(CH_3OH)]$ moity is surrounded by an N_2O_2 coordination sphere (N6, N7, O11 and O14) of the completely deprotonated ligand $(L^1)^-$ unit, one oxygen atom (O17) from the coordinated methanol molecule. In order to get the geometries adopted by Cu1 and Cu2, the τ values were estimated to be $\tau_1 = 0.00017$ and $\tau_2 = 0.0062$ [56,57], respectively.

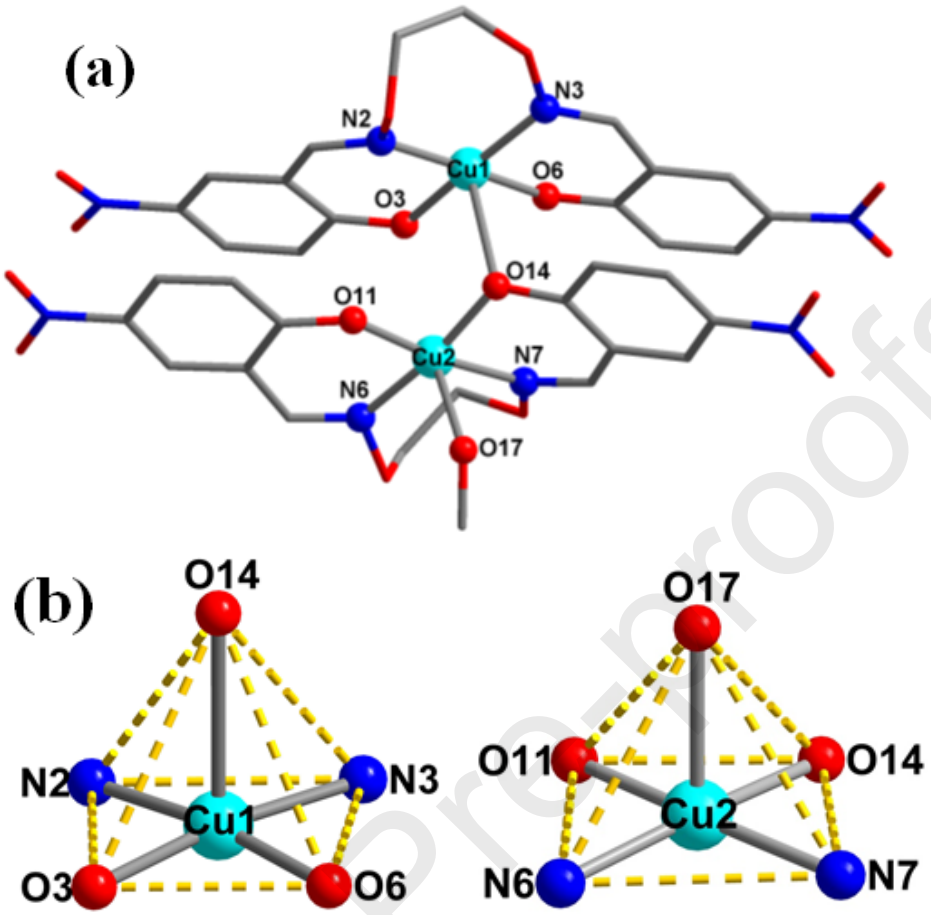

Fig. 3. (a) Molecule structure and atom numberings of the complex **1** (hydrogen atoms are omitted for clarity). (b) Coordination polyhedra for Cu(II) atoms of the complex **1**.

As illustrated in Fig. 4. In the crystal structure of the complex **1**, there are two pairs of intra-molecular hydrogen bonding interactions (C25-H25B···O3 and C33-H33A···O12) and ten pairs of inter-molecular hydrogen bonding interactions (O17-H17···O11, O17-H17···O17, O18-H18A···O5, C7-H7···O1, C9-H9A···O6, C10-H10A···O8, C23-H23···O9, C24-H24A···O9, C24-H24B···O12 and C33-H33B···O4), as shown in Fig. 5. The intra-molecular and inter-molecular hydrogen bonding interactions are summarized in Table 5. As shown in Fig. 5(a), the supra-molecular structure of the complex **1** is linked further by inter-molecular hydrogen bonding interactions (C9-H9A···O6 and C23-H23···O9), the hydrogen bond interactions play a major role in the building of the complex **1** [58]. At the same time, in Fig. 5(b), through the inter-molecular hydrogen bonding interactions, this network

structure is connected to each other to gain an infinite three-dimensional supra-molecular structure [59,60].

Table 3

Selected bond lengths (Å) and angles (°) for the complex **1**.

Bond	Dist.	Bond	Dist.	Bond	Dist.
Cu1-O3	1.945(4)	Cu1-N3	2.020(5)	Cu2-N6	1.964(5)
Cu1-O6	1.914(4)	Cu2-O11	1.945(4)	Cu2-N7	2.035(5)
Cu1-O14	2.600(4)	Cu2-O14	1.927(4)		
Cu1-N2	1.947(5)	Cu2-O17	2.278(4)		
Bond	Angles	Bond	Angles	Bond	Angles
O3-Cu1-O6	84.26(16)	O14-Cu1-N2	93.60(18)	O14-Cu2-O17	92.05(17)
O3-Cu1-O14	92.94(15)	O14-Cu1-N3	90.97(18)	O14-Cu2-N6	172.18(19)
O3-Cu1-N2	88.84(17)	N2-Cu1-N3	98.03(19)	O14-Cu2-N7	87.05(17)
O3-Cu1-N3	171.87(19)	O11-Cu2-O14	86.38(15)	O17-Cu2-N6	94.3(2)
O6-Cu1-O14	91.06(15)	O11-Cu2-O17	92.95(17)	O17-Cu2-N7	90.78(19)
O6-Cu1-N2	171.86(19)	O11-Cu2-N6	88.67(17)	N6-Cu2-N7	97.48(19)
O6-Cu1-N3	88.55(18)	O11-Cu2-N7	172.55(18)		

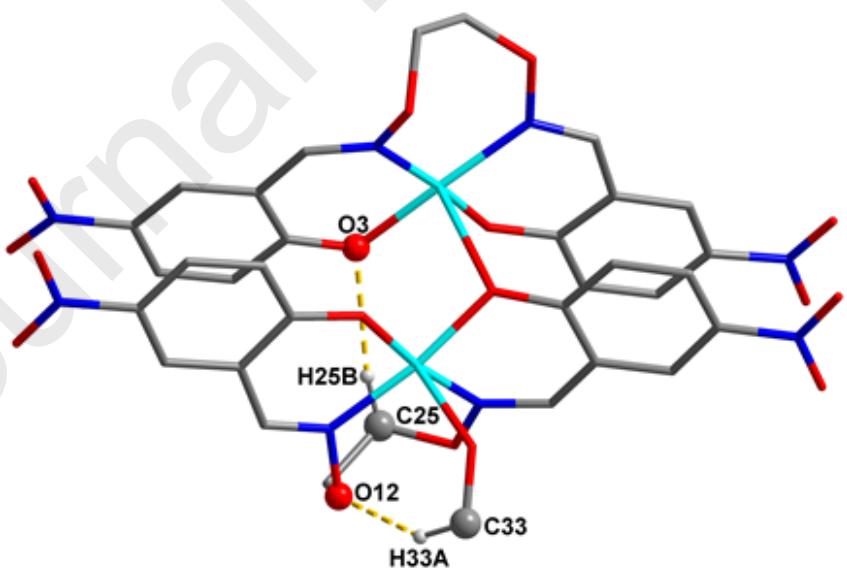

Fig. 4. View of the intra-molecular hydrogen bondings of the complex **1** unit (for clarity purpose, hydrogen atoms are omitted except those forming hydrogen bonds).

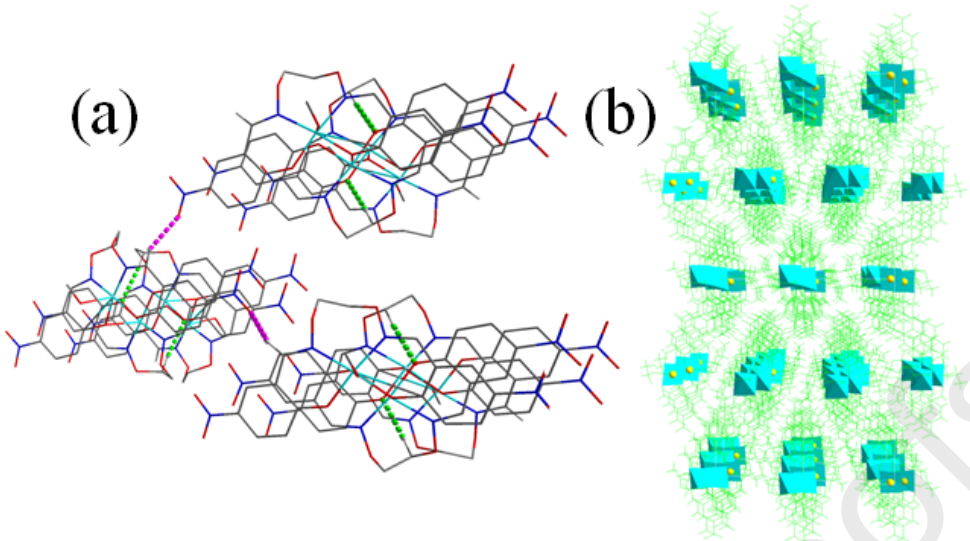

Fig. 5. View of the inter-molecular hydrogen bonding interactions of the complex **1**.

Table 4

Selected bond lengths (Å) and angles (°) for the complex **2**.

Bond	Dist.	Bond	Dist.	Bond	Dist.
Cu1-O2	1.917(6)	Cu1-N1	1.973(5)	Cu1-O2$^{\#1}$	1.917(6)
Cu1-N1$^{\#1}$	1.973(5)				
Bond	**Angles**	**Bond**	**Angles**	**Bond**	**Angles**
O2-Cu1-N1	89.1(2)	O2-Cu1-O2$^{\#1}$	180	O2-Cu1-N1$^{\#1}$	90.9(2)
O2$^{\#1}$-Cu1-N1	90.9(2)	N1-Cu1-N1$^{\#1}$	180	O2$^{\#1}$-Cu1-N1$^{\#1}$	89.1(2)

Symmetry transformations used to generate equivalent atoms: $^{\#1}$2-x,-y,-z

Table 5

Putative hydrogen bond interactions (Å,°) for the complex **1**.

D–X···A	d(D–X)	d(X···A)	d(D···A)	∠D–X···A	Symmetry code
O17–H17···O11	1.05	1.98	2.767(6)	129	1-*x*,1-*y*,1-*z*
O17–H17···O17	1.05	2.57	3.492(6)	147	1-*x*,1-*y*,1-*z*
O18–H18A···O5	0.84	2.46	3.220(8)	152	x,1/2-y,-1/2+z
C7–H7···O1	0.95	2.27	3.193(7)	164	x,3/2-y,1/2+z
C9–H9A···O6	0.99	2.38	3.365(7)	175	2-x,1-y,1-z
C10–H10A···O8	0.95	2.41	3.274(7)	151	x,1/2-y,1/2+z
C23–H23···O9	0.95	2.48	3.119(7)	124	x,3/2-y,-1/2+z
C24–H24A···O9	0.99	2.45	3.374(7)	155	x,3/2-y,-1/2+z
C24–H24B···O12	0.99	2.59	3.312(7)	130	1-x,1-y,-z
C25–H25B···O3	0.99	2.46	3.438(7)	171	

C33–H33A···O12	0.98	2.53	3.362(8)	142	
C33–H33B···O4	0.98	2.33	3.168(8)	142	1-x,1-y,1-z

*3.4.2. Crystal structure of the complex **2***

As shown in Fig. 6. The Cu(II) complex **2** has a symmetrical mononuclear structure. In the crystal structure of the complex **2**, the four-coordinated Cu(II) atom (Cu1) lies in the N_2O_2 coordination sphere (N1, N1$^{\#1}$, O2 and O2$^{\#1}$) of two completely deprotonated ligand $(L^2)^-$ units, forming a planar quadrilateral geometric configuration.

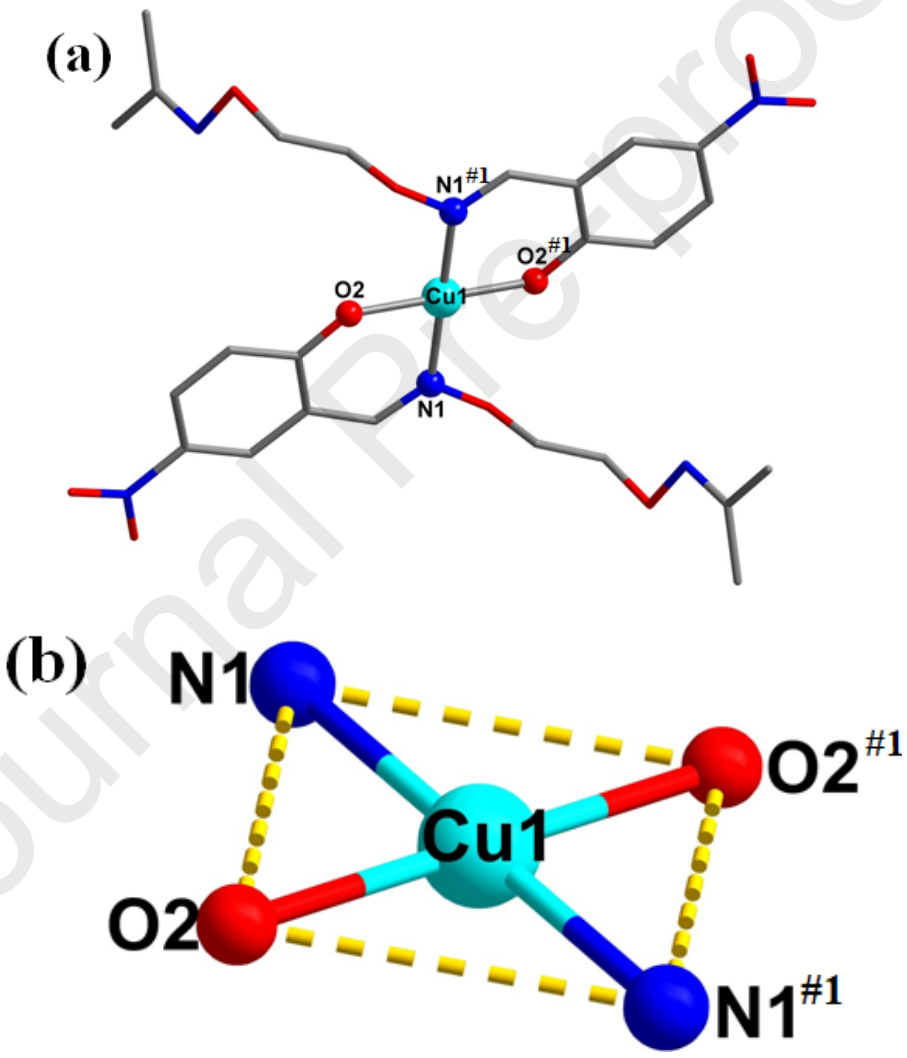

Fig. 6. (a) Molecule structure and atom numberings of the complex **2** (hydrogen atoms are omitted for clarity). (b) Coordination polyhedron for Cu(II) atom of the complex **2**.

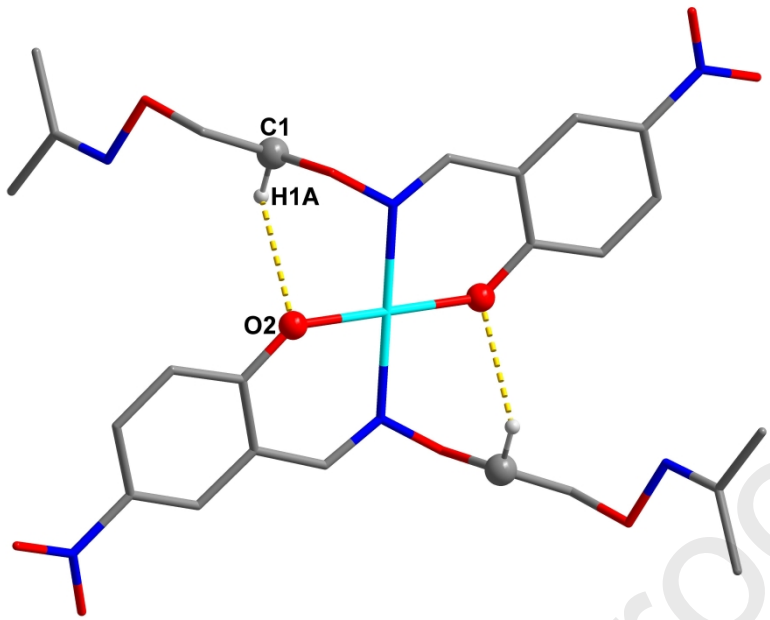

Fig. 7. View of the intra-molecular hydrogen bondings of the complex **2** unit (for clarity purpose, hydrogen atoms are omitted except those forming hydrogen bonds).

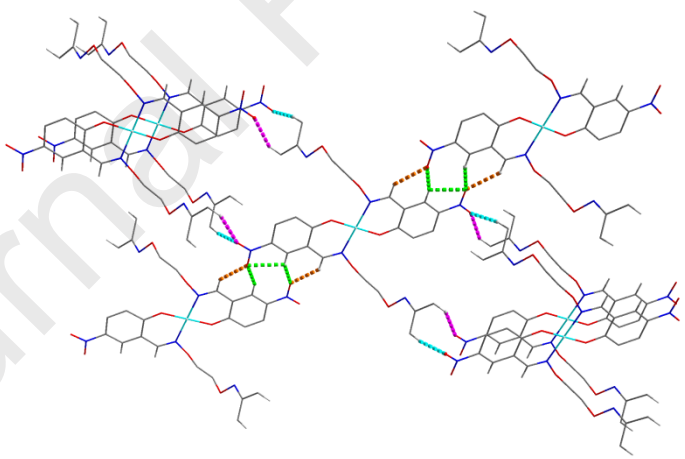

Fig. 8. View of the inter-molecular hydrogen bonding interactions of the complex **2**.

As illustrated in Table 6 and Fig. 7, in the crystal structure of the complex **2**, there are only one pair of intra-molecular hydrogen bonding (C1-H1A···O2) and four pairs of inter-molecular hydrogen bonding interactions (C3-H3···O3, C6-H6···O3, C10-H10B···O5 and C11-H11B···O5) (Fig. 7 and Fig. 8). The intra-molecular and

inter-molecular hydrogen bonding interactions are summarized in Table 6. As shown in Fig. 8, the supra-molecular structure of the Cu(II) complex **2** is linked further by inter-molecular hydrogen bonding interactions (C3-H3···O3, C6-H6···O3, C10-H10B···O5 and C11-H11B···O5), which performs a crucial role in constructing and stabilizing 2D supra-molecular chain structure.

Table 6

Putative hydrogen bond interactions (Å,°) for the complex **2**.

D–X···A	d(D–X)	d(X···A)	d(D···A)	∠D–X···A	Symmetry code
C1–H1A···O2	0.97	2.57	3.082(10)	113	-x,1-y,1-z
C3–H3···O3	0.93	2.55	3.334(8)	142	-x,1-y,2-z
C6–H6···O3	0.93	2.38	3.210(10)	149	-x,1-y,2-z
C10–H10B···O5	0.96	2.58	3.336(10)	136	-1+x,1+y,-1+z
C11–H11B···O5	0.96	2.57	3.500(10)	163	x,1+y,-1+z

3.5. Hirshfeld surfaces analyses

The Hirshfeld surfaces [61] of the complexes **1** and **2** are illustrated in Fig. 9, showing surfaces that have been mapped over d_{norm} and the corresponding location in shape index exists the complementary region of red concave surface surrounded by receptors and the blue convex surface surrounding receptors, further proving that such hydrogen bonding exists. As for the large amount of white region in d_{norm} surfaces, it is suggested that there is a weaker and farther contact between molecules, rather than hydrogen bondings. Fig. 9. shows two-dimensional [62] Hirshfeld surface generation map, the blue region represents the distribution of different interactions of the complexes **1** and **2**.

As shown in Fig. 10a, about the complex **1**, the H···H interactions appear at (0.91Å, 0.91Å) and accounting for 52.6% of the total area of Hirshfeld surfaces. The C···H/H···C interactions in the range of (1.65Å, 1.65Å) and appears as a pair of symmetrical wings, accounting for 4.2% of the total area of Hirshfeld surfaces. The proportions of O···H/H···O interactions comprise 46.2% of the total Hirshfed surfaces for each molecule of the complex **1**. As shown in Fig. 10b, about the complex **2**, the

interactions of H···H appeared at (1.15Å, 1.15Å) accounting for 50.7% of the total area of Hirshfeld surfaces. The C···H/H···C interactions in the range of (1.76Å, 1.76Å) accounting for 6.2% of the total area of Hirshfeld surfaces. The proportions of O···H/H···O interactions comprise 27.8% of the total Hirshfed surfaces for each molecule of the complex **2**. It is because of the existence of these weaker hydrogen bonds that the complexes **1** and **2** can be stable.

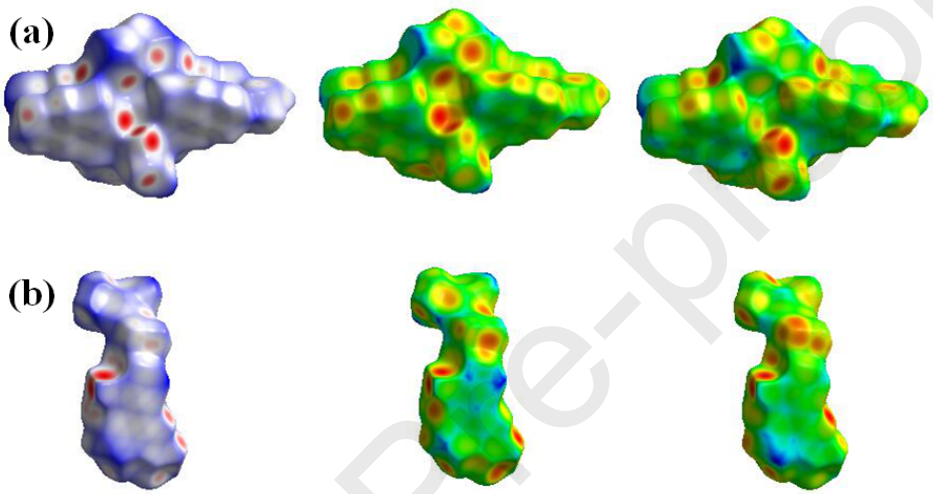

Fig. 9. Hirshfeld surfaces analyses mapped with curvedness, d_{norm} and shape index of the complexes **1** and **2**.

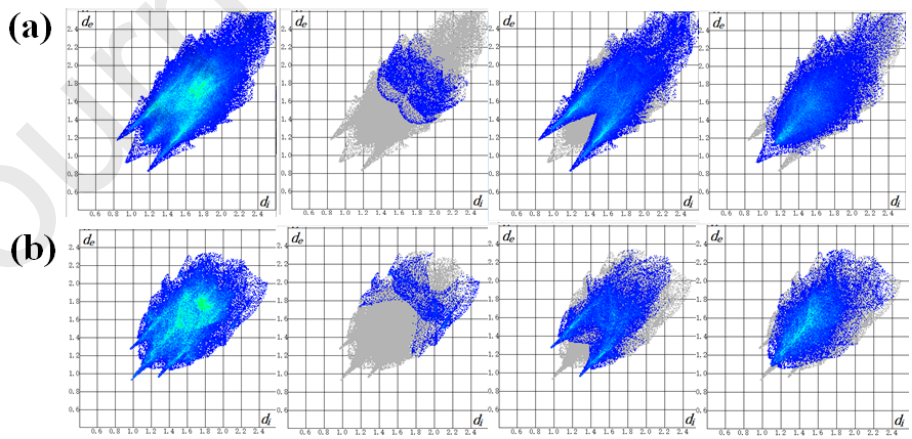

Fig. 10. Fingerprint plots of the complex **1** (a) and complex **2** (b): full and resolved into full and resolved into C···H, O···H and H···H contacts showing the percentages of contacts contributed to the total Hirshfeld surface area of molecule.

Conclusion

In summary, we have reported the successful syntheses and characterizations of two newly designed transition metal(II) complexes $[\{Cu(L^1)\}_2(CH_3OH)]\cdot CH_3OH$ (**1**) and $[Cu(L^2)_2]$ (**2**) derived from a half-salamo-based ligand HL. The penta-coordinated Cu(II) ions (Cu1 and Cu2) in the complex **1** form slightly distorted tetragonal pyramidal geometric configurations. The supra-molecular structure of the complex **1** is formed by inter-molecular hydrogen bonding interactions, resulting in a self-assembled infinite 3D supra-molecular network. The four-coordinated Cu(II) ion (Cu1) in the complex **2** forms a planar quadrilateral geometric configuration. The supra-molecular structure of the complex **2** is formed by inter-molecular hydrogen bonding inter-actions, resulting in a self-assembled infinite 2D supra-molecular network. The Hirshfeld surfaces and 2D fingerprint plots can explain the atom pair contacts of the crystal, which can quantify the intermolecular interactions. The Cu(II) complexes **1** and **2** display lower photoluminescence compared with HL, emission intensities of the Cu(II) complexes **1** and **2** evidently are reduced, indicating that the fluorescence characteristics were affected by the introduction of Cu(II) ions, as a result, the fluorescence intensity gradually weakens during the process from the ligand HL to the Cu(II) complexes. These transitions may be related to the coordination of the ligand HL and the Cu(II) ions, which allows the ligand to develop towards a more stable complexes.

Appendix A. Supplementary data

CCDC–1990139 and 1990138 contains the supplementary crystallographic data for the Cu(II) complexes **1** and **2**. These data can be obtained free of charge via www.ccdc.cam.ac.uk/conts/retrieving.html, or from the Cambridge Crystallographic Data Centre, 12 Union Road, Cambridge CB2 1EZ, UK (Telephone: +44–01223–762910; Fax: +44–1223–336033; or E-mail: deposit @ccdc.cam.ac.uk).

Acknowledgements

This work was supported by the National Natural Science Foundation of China (21968032), Special Funds for Discipline Construction of Gansu Agricultural University (LXYXK201801) and the Program for Excellent Team of Scientific Research in Lanzhou Jiaotong University (201706), which are gratefully acknowledged.

References

[1] P. Jeslin Kanaga Inba, B. Annaraj, S. Thalamuthu, M.A. Neelakantan, Spectrochim. Acta Part A 104 (2013) 300.

[2] H.L. Wu, G.L. Pan, Y.C. Bai, H. Wang, J. Kong, F.R. Shi, Y.H. Zhang, X.L. Wang, Res. Chem. Intermed. 41 (2015) 3375.

[3] Y.A. Liu, C.Y. Wang, M. Zhang, X.Q. Song, Polyhedron 127 (2017) 278.

[4] X.Y. Dong, Q.P. Kang, X.Y. Li, J.C. Ma, W.K. Dong, Crystals 8 (2018) 139.

[5] I. Cacelli, L. Carbonaro, P. La Pegna, Eur. J. Inorg. Chem. (2002) 1703.

[6] J. Reglinski, S. Morris, D.E. Stevenson, Polyhedron 21 (2002) 2167.

[7] F.Z. Chiboub Fellah, S. Boulefred, A. Chiboub Fellah, B. El Rez, C. Duhayon, J.-P. Sutter, Inorg. Chim. Acta 439 (2016) 24.

[8] Y. Zhang, Y.Q. Pan, M. Yu, X. Xu, W.K. Dong, Appl. Organomet. Chem. 33 (2019) e5240.

[9] H. Miyasaka, N. Matsumoto, H. Okawa, N. Re, E. Gallo, C. Floriani, J. Am. Chem. Soc. 118 (1996) 981

[10] N.S. Venkataramanan, G. Kuppuraj, S. Rajagopal, Coord. Chem. Rev. 249 (2005) 1249.

[11] Z. Abbasi, M. Behzad, A. Ghaffari, H.A. Rudbari, G. Bruno, Inorg. Chim. Acta 414 (2014) 78.

[12] L.Q. Chai, L. Zhou, K.Y. Zhang, H.S. Zhang, Appl. Organomet. Chem. (2018) e4576.

[13] L.W. Zhang, X.Y. Li, Q.P. Kang, L.Z. Liu, J.C. Ma, W.K. Dong, Crystals 8 (2018) 173.

[14] Q.P. Kang, X.Y. Li, Q. Zhao, J.C. Ma, W.K. Dong, Appl. Organomet. Chem. 32 (2018) e4379.

[15] L. Wang, Z.L. Wei, Z.Z. Chen, C. Liu, W.K. Dong, Y.J. Ding, Microchem. J. 155 (2020) 104801.

[16] J. Li, H.J. Zhang, J. Chang, H.R. Jia, Y.X. Sun, Y.Q. Huang, Crystals 8 (2018) 176.

[17] J.L. Arthur, K.S. Min, J.S. Miller, Journal of Magnetism and Magnetic Materials 489 (2019) 165375.

[18] Z.L. Ren, J. Hao, P. Hao, X.Y. Dong, Y. Bai, W.K. Dong, Z. Naturforsch. B 73 (2018) 203.

[19] A.K. Asatkar, M. Tripathi, S. Panda, R. Pande, S.S. Zade, Spectrochim. Acta Part A. 171 (2017) 18.

[20] X.Y. Dong, Q. Zhao, Z.L. Wei, H.R. Mu, H. Zhang, W.K. Dong, Molecules 23 (2018) 1006.

[21] C.C. Black, A.E.V. Gorden, Tetrahedron Lett. 59(2018) 803.

[22] Y. Deawati, D. Onggo, I. Mulyani, I.Hastiawan, D. Kurnia, P. Lönnecke, S. Schmorl, B. Kersting, E. Hey-Hawkins, Inorg. Chim. Acta 482 (2018) 353.

[23] Q.P. Kang, X.Y. Li, L. Wang, Y. Zhang, W.K. Dong, Appl Organomet. Chem. 33 (2019) e5013.

[24] A. Bhunia, M.A. Gotthardt, M. Yadav, M.T. Gamer, A. Eichhoefer, W. Kleist, P.W. Roesky, Chem. Eur. J. 19 (2013) 1986.

[25] S. Akine, T. Taniguchi, W.K. Dong, T. Nabeshima, J. Org. Chem. 70 (2005) 1704.

[26] Q. Zhao, X.X. An, L.Z, Liu, W.K. Dong, Inorg. Chim. Acta. 490 (2019) 6.

[27] F. Wang, L.Z. Liu, L. Gao, W.K. Dong, Spectrochim. Acta Part A. 203 (2018) 56.

[28] Y.D. Peng, F. Wang, L. Gao, W.K. Dong, J. Chin. Chem. Soc. 65 (2018) 893.

[29] L.W. Zhang, L.Z. Liu, F. Wang, W.K. Dong, Molecules 23 (2018) 1141.

[30] X.X. An, Q. Zhao, H.R. Mu, W.K. Dong, Crystals 9 (2019) 101.

[31] L.Z. Liu, M. Yu, X.Y. Li, Q.P. Kang, W.K. Dong, Chin. J. Inorg. Chem. 35 (2019) 1283.

[32] Y.Q. Pan, X. Xu, Y. Zhang, Y. Zhang, W.K. Dong, Spectrochim. Acta A, 229 (2020) 117917.

[33] Q.P. Kang, X.Y. Li, Z.L. Wei, Y. Zhang, W.K. Dong, Polyhedron 165 (2019) 38.

[34] S. Akine, S. Kagiyama, T. Nabeshima, Inorg. Chim. 46 (2007) 9525.

[35] Y. Zhang, M. Yu, Y.Q. Pan, Y. Zhang, L. Xu, W.K. Dong, Appl. Organomet. Chem. 34 (2020) e5442.

[36] H.J. Zhang, J. Chang, H.R. Jia, Y.X. Sun, Chinese J. Inorg. Chem. 34 (2018) 2261.

[37] X.Y. Dong, Q. Zhao, Q.P. Kang, X.Y. Li, W.K. Dong, Crystals 8 (2018) 230.

[38] C. Liu, X.X. An, Y.F. Cui, K.F. Xie, W.K. Dong, Appl. Organomet. Chem. 34 (2020) e5272.

[39] H.R. Jia, J. Chang, H.J. Zhang, J. Li, Y.X. Sun, Crystals 8 (2018) 272.

[40] J. Hao, X.Y. Li, Y. Zhang, W.K. Dong, Materials 11 (2018) 523.

[41] J. Chang, H.J. Zhang, H.R. Jia, Y.X. Sun, Chinese J. Inorg. Chem. 34 (2018) 2097.

[42] L.W. Zhang, Y. Zhang, Y.F. Cui, M. Yu, W.K. Dong, Inorg. Chim. Acta 506 (2020) 119534.

[43] Z.L. Wei, L. Wang, J.F. Wang, W.T. Guo, Y. Zhang, W.K. Dong, Spectrochim. Acta A, 228 (2020) 117775.

[44] D.W. Dixon, R.H. Weiss, J. Org. Chem. 49 (1984) 4487.

[45] G.M. Sheldrick, SHELXS-97, program for the solution and the refinement of crystal structures, University of Gottingen, Germany. 1997.

[46] Y.X. Sun, Y.Q. Pan, X. Xu, Y. Zhang, Crystals 9 (2019) 607.

[47] L.Z. Liu, L. Wang, M. Yu, Q. Zhao, Y. Zhang, Y.X. Sun, W.K. Dong, Spectrochim. Acta Part A. 222 (2019) 117209.

[48] Y. Zhang, L.Z. Liu, Y.D. Peng, N. Li, W.K. Dong, Transit. Met. Chem. 44 (2019) 627.

[49] S. Akine, Y. Morita, F. Utsuno, T. Nabeshima, Inorg. Chem. 48 (2009) 10670.

[50] X.Y. Li, Q.P. Kang, C. Liu, Y. Zhang , W.K. Dong, New J. Chem. 43 (2019) 4605.

[51] S. Akine, T. Taniguchi, T. Saiki, T. Nabeshima, J. Am. Chem. Soc. 127 (2005) 540.

[52] S. Akine, T. Taniguchi, T. Nabeshima, Inorg. Chim. 47 (2008) 3255.

[53] S. Akine, S. Kagiyama, T. Nabeshima, Inorg. Chim. 49 (2010) 2141.

[54] S. Akine, T. Taniguchi, T. Nabeshima, Tetrahedron Lett. 47 (2006) 8419.

[55] M. Yu, H.R. Mu, L.Z. Liu, N. Li, Y. Bai, X.Y. Dong, Chin. J. Inorg. Chem. 35 (2019) 1109.

[56] A.W. Addison, T.N. Rao, J. Reedijk, J. Chem. Soc., Dalton Trans. 7 (1984) 1349.

[57] T. Konno, K. Tokuda, J. Sakurai, Bull. Chem. Soc. Jpn. 73 (2000) 2767.

[58] J. Bernstein, R.E. Davis, L. Shimoni, N.L. Chang, Angew. Chem. Int. Ed. Engl. 34 (1995) 1555.

[59] Y. Q. Pan, Y. Zhang, M. Yu, Y. Zhang, L. Wang, Appl. Organomet. Chem. 34 (2020) e5441.

[60] X.X. An, C. Liu, Z.Z. Chen, K.F. Xie, Y. Zhang, Crystals 9 (2019) 602.

[61] M.A. Spackman, J.J. McKinnon, D. Jayatilaka, Cryst. Eng. Commu. 10 (2008) 377.

[62] A.L. Rohl, M. Moret, W. Kaminsky, K. Claborn, J.J. Mckinnon, B. Kahr, Cryst. Growth Des. 8 (2008) 4517.

Author Statement: The authors declare no competing financial interests.

[63]

Conflicts of Interest: The authors declare no competing financial interests.

[64]

Graphical Abstract

Two novel Cu(II) complexes, $[\{Cu(L^1)\}_2(CH_3OH)]\cdot CH_3OH$ (**1**) and $[Cu(L^2)_2]$ (**2**) derived from a half-salamo-based N_2O-donor ligand (HL: 2-[*O*-(1-ethyloxyamide)]oxime-4-nitrophenol) were synthesized and characterized by elemental analyses, infrared spectroscopy, ultraviolet-visible absorption spectroscopy, X-ray single crystal diffraction and Hirshfeld surfaces analyses.

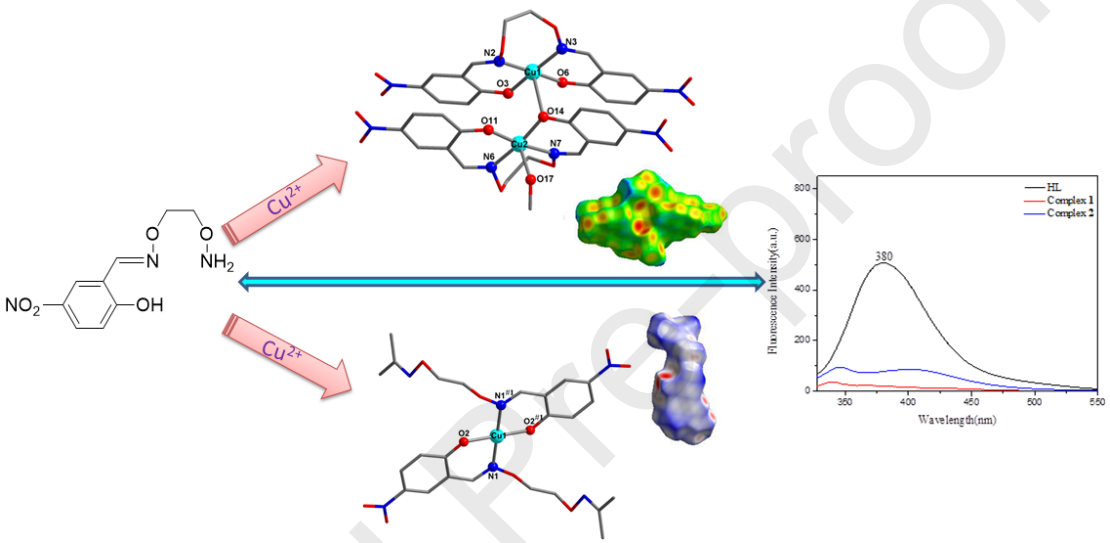

[65]

Highlights:

• Dinuclear and mononuclear Cu(II) complexes were synthesized and characterized

structurally.

• The crystal structures of the Cu(II) complexes are interesting.

• Hirshfeld surfaces and luminescences of the Cu(II) complexes were investigated.

[66]